ARTICLES

Driving fast-spiking cells induces gamma rhythm and controls sensory responses

Jessica A. Cardin[1,2]*, Marie Carlén[3,4]*, Konstantinos Meletis[3,4], Ulf Knoblich[1], Feng Zhang[5], Karl Deisseroth[5], Li-Huei Tsai[3,4,6] & Christopher I. Moore[1]

Cortical gamma oscillations (20−80 Hz) predict increases in focused attention, and failure in gamma regulation is a hallmark of neurological and psychiatric disease. Current theory predicts that gamma oscillations are generated by synchronous activity of fast-spiking inhibitory interneurons, with the resulting rhythmic inhibition producing neural ensemble synchrony by generating a narrow window for effective excitation. We causally tested these hypotheses in barrel cortex *in vivo* by targeting optogenetic manipulation selectively to fast-spiking interneurons. Here we show that light-driven activation of fast-spiking interneurons at varied frequencies (8−200 Hz) selectively amplifies gamma oscillations. In contrast, pyramidal neuron activation amplifies only lower frequency oscillations, a cell-type-specific double dissociation. We found that the timing of a sensory input relative to a gamma cycle determined the amplitude and precision of evoked responses. Our data directly support the fast-spiking-gamma hypothesis and provide the first causal evidence that distinct network activity states can be induced *in vivo* by cell-type-specific activation.

Brain states characterized by rhythmic electrophysiological activity have been studied intensively for more than 80 years[1,2]. Because these brain rhythms are believed to be essential to information processing, many theories have been proposed to explain their origin, with several emphasizing the activity of neural subtypes. One of the strongest cases made so far for the importance of a specific cell type in rhythm induction is the suggested role of fast-spiking (FS) interneurons in gamma oscillations[3–6]. Networks of FS cells connected by gap junctions[7,8] provide large, synchronous inhibitory postsynaptic potentials (IPSPs) to local excitatory neurons[9,10]. Computational modelling indicates that this synchronous activity is sufficient to induce 20−80-Hz oscillations that are stabilized and regulated by fast excitatory feedback from pyramidal neurons[11,12]. Cortical recordings *in vivo* show sensory-evoked gamma oscillations in the local field potential (LFP) and phase-locked firing of excitatory pyramidal cells, indicating entrainment of excitatory neurons to rhythmic inhibitory activity[9,13–15]. Despite considerable study of cortical oscillations and the importance of understanding their origins, induction of a given network state by stimulation of specific neural cell types *in vivo* has not previously been possible.

Cell-type-specific expression of channelrhodopsin-2

To test directly the hypothesis that FS interneuron activity in an *in vivo* cortical circuit is sufficient to induce gamma oscillations, we used the light-sensitive bacteriorhodopsin *Chlamydomonas reinhardtii* channelrhodopsin-2 (ChR2), a cation channel activated by ~470 nm blue light[16,17]. We targeted expression of ChR2 specifically to parvalbumin-positive fast-spiking (FS-PV$^+$) interneurons by injecting the adeno-associated viral vector double-floxed inverted open reading frame *ChR2−mCherry* (AAV DIO *ChR2−mCherry*), with Cre-dependent expression of ChR2, into PV−Cre knock-in mice (Fig. 1a, Supplementary Figs 1 and 2 and Methods)[18,19]. Six days after virus injection into barrel cortex of adult PV−Cre mice, ChR2−mCherry expression covered an anterioposterior distance of up to 1,740 μm (1,695 ± 57.4 μm, mean ± s.d., $n = 3$), resulting in robust labelling of PV$^+$ interneurons across cortical layers (Fig. 1b). The labelling efficiency of AAV DIO *ChR2−mCherry* varied over distance from the injection site; close to the centre of the injection, >97% of the PV$^+$ interneurons expressed ChR2−mCherry. Immunohistochemistry confirmed that 96.7 ± 1.0% (mean ± s.d., $n = 4{,}234$ ChR2−mCherry$^+$ neurons, 4 animals) of the ChR2−mCherry$^+$ neurons expressed PV (Fig. 1d, e and Supplementary Fig. 2), and almost all expressed the inhibitory neurotransmitter GABA (γ-aminobutyric acid; Supplementary Fig. 3)[20–23]. Expression of ChR2−mCherry was not induced after injection of AAV DIO *ChR2−mCherry* into wild-type mice (data not shown) or *in vitro* in the absence of Cre (see Supplementary Methods; data not shown).

In experiments targeting excitatory neurons, AAV DIO *ChR2−mCherry* was injected into the barrel cortex of adult CW2 (ref. 24) mice, which express Cre from the *αCamKII* (also known as *Camk2a*) promoter ('αCamKII−Cre mice'), inducing recombination in excitatory neurons in cortex[24]. Robust ChR2−mCherry expression was observed in excitatory neurons in a laminar profile corresponding to the Cre expression pattern (Fig. 1c and Supplementary Fig. 4)[24]. At least 50% of the αCamKII$^+$ neurons in layer 2/3 expressed ChR2−mCherry (913 of 1,638 cells in a total area of 8.4×10^6 μm^3) close to the injection site, covering an anterioposterior distance of 1,560 ± 154.9 μm (mean ± s.d., $n = 3$). Immunohistochemical analysis revealed that 100 ± 0% (mean ± s.d., $n = 4{,}024$ ChR2−mCherry$^+$ neurons, 4 animals) of the ChR2−mCherry-expressing neurons were immuno-negative for PV (Fig. 1f, g and Supplementary Fig. 2), and 100 ± 0% expressed the neuronal marker NeuN (data not shown).

FS activation suppresses local sensory responses

We recorded light-activated FS and regular spiking (RS) single units in layers 2/3 and 4 of barrel cortex in PV−Cre ($n = 64$ FS cells in 15 animals) and αCamKII−Cre ($n = 56$ RS cells in 7 animals) mice. We

[1]McGovern Institute for Brain Research and Department of Brain and Cognitive Sciences, MIT, Cambridge, Massachusetts 02139, USA. [2]Department of Neuroscience, University of Pennsylvania, Philadelphia, Pennsylvania 19104, USA. [3]Picower Institute for Learning and Memory, Department of Brain and Cognitive Sciences, MIT, Cambridge, Massachusetts 02139, USA. [4]Stanley Center for Psychiatric Research, Broad Institute of Harvard and Massachusetts Institute of Technology, Cambridge, Massachusetts 02139, USA. [5]Department of Bioengineering, Stanford University, Stanford, California 94305, USA. [6]Howard Hughes Medical Institute, Cambridge, Massachusetts 02139, USA.
*These authors contributed equally to this work.

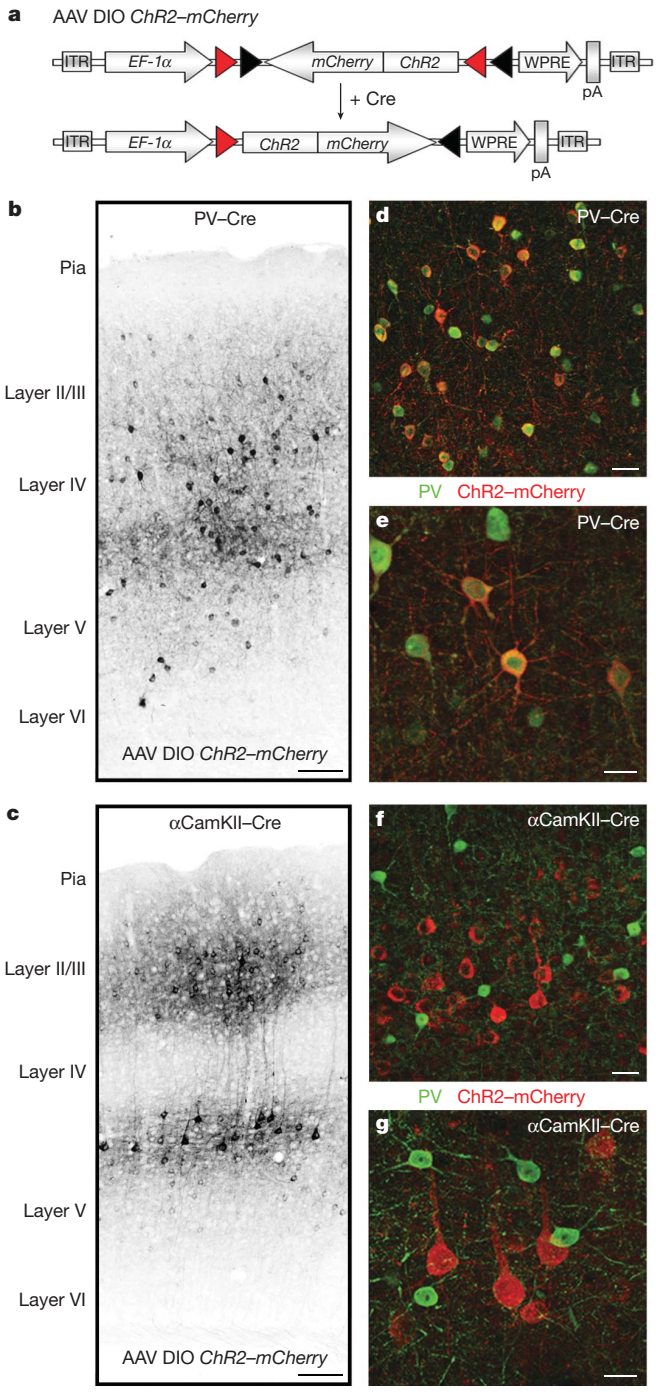

Figure 1 | AAV DIO *ChR2−mCherry* gives Cre-dependent and cell-type-specific expression of light-activated channels *in vivo*. **a**, AAV DIO *ChR2−mCherry* with Cre-dependent expression of ChR2 produced cell-type-specific targeting of light-activated channels. In the presence of Cre, *ChR2−mCherry* is inverted into the sense direction and expressed from the *EF-1α* (*EEF1A1*) promoter. ITR, inverted terminal repeat; pA, poly(A); WPRE, woodchuck hepatatis B virus post-transcriptional element. **b**, ChR2−mCherry was robustly expressed in PV^+ interneurons in barrel cortex of adult PV−Cre mice. **c**, A corresponding injection in αCamKII−Cre mice resulted in exclusive labelling of excitatory neurons. **d**, **e**, ChR2−mCherry expression in PV−Cre mice was confined to cells expressing PV. **e**, PV^+ cells with ChR2−mCherry expression and typical FS interneuron morphology. **f**, **g**, ChR2−mCherry expression in αCamKII−Cre mice is confined to neurons immuno-negative for PV. **g**, ChR2−mCherry-expressing cells with typical pyramidal neuron morphology. Scale bars: **b**, **c**, 100 μm; **d**–**g**, 25 μm.

did not observe light activation of layer 5 FS cells ($n = 12$ sites in 7 animals). Barrel cortex, which processes information from the rodent vibrissae (whiskers), was targeted as a well-defined model of basic sensory cortical function. In agreement with the immunohistological results, the action potential shapes of the neurons activated by light pulses were differentiated into two discrete populations based on mouse type: PV−Cre/FS and αCamKII−Cre/RS ($P < 0.01$; Fig. 2a).

To confirm the activation of inhibitory interneurons and their postsynaptic impact on excitatory neurons, we performed *in vivo* intracellular recordings of RS cells in barrel cortex of PV−Cre mice ($n = 5$). We found that a 1-ms light pulse was sufficient to evoke large, fast IPSPs, confirming direct synaptic inhibition of RS cells by light-activated FS cells (Fig. 2b). The latencies of the presynaptic light-evoked FS spikes agreed well with the onset times of the post-synaptic IPSPs, with FS spikes preceding IPSP onset by 0.5 to 0.75 ms (Fig. 2c). Both the time to peak and the peak timing variability of the evoked IPSPs decreased with increasing light pulse power (Fig. 2c). Mean IPSP peak amplitude at membrane potentials of −55 to –60 mV was 2.7 ± 1.0 mV. The mean reversal potential of the evoked IPSPs (see Supplementary Methods) was –67.6 ± 1.9 mV, indicating a $GABA_A$-mediated Cl^- conductance characteristic of FS synapses. Consistent with IPSP induction, activation of FS cells blocked vibrissa-evoked responses in neighbouring RS cells (Fig. 2d, e; $n = 6$ sites in 5 PV−Cre mice).

FS activation generates gamma oscillations

A strong prediction of the FS-gamma hypothesis is that synchronously active FS cells are sufficient for gamma induction. This hypothesis

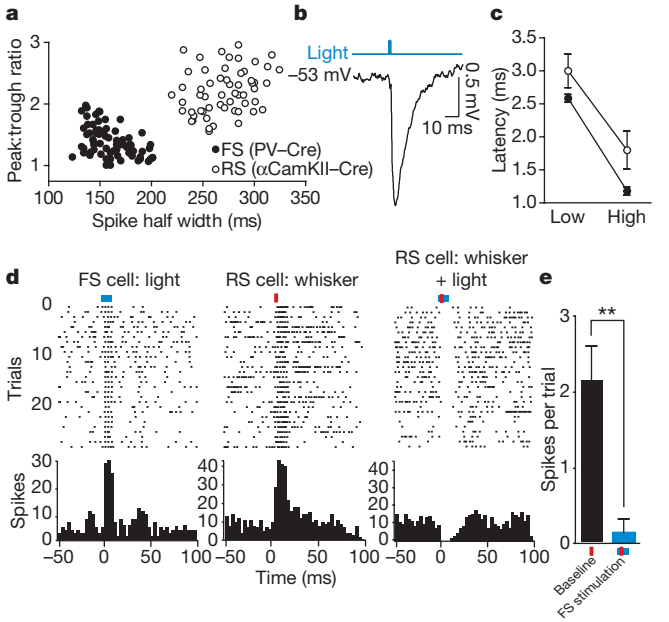

Figure 2 | Light-evoked activity in FS-PV^+ inhibitory interneurons suppresses sensory processing in nearby excitatory neurons. **a**, Light-activated RS and FS cells recorded in layers 2/3 and 4 of barrel cortex in PV−Cre and αCamKII−Cre mice, respectively, formed two discrete overall populations based on waveform properties. **b**, Intracellular *in vivo* recording of an RS cell in a PV−Cre animal. A 1-ms pulse of blue light at low power evoked an IPSP with a sharp onset. **c**, The latency to light-activated FS spikes (filled circles) agreed well with the onset latency of the resulting IPSPs (open circles). The IPSP time to peak decreased with increasing power (low power: 46 mW mm^{-2}; high power: 68 mW mm^{-2}). **d**, Sustained activation of FS inhibitory interneurons eliminated sensory responses in nearby RS neurons. A layer 2/3 FS cell was reliably activated by a 10-ms light pulse (blue line; left panel). An RS cell recorded on the same tetrode responded to vibrissa deflection (red bar; centre panel). Activation of inhibitory activity simultaneously with vibrissa deflection eliminated the RS sensory response (right panel). **e**, Mean RS vibrissa response decreased significantly in the presence of increased FS cell activity. $^{**}P < 0.01$; error bars, mean ± s.e.m.

predicts that light pulses presented at a broad range of frequencies should reveal a selective peak in enhancement of the LFP, a measure of synchronous local network activity[25], when FS cells are driven in the gamma range.

To test this hypothesis, we drove cortical FS cell spiking in virus-transduced PV−Cre mice at a range of frequencies (8−200 Hz) with 1-ms light pulses. Light pulses in the gamma range (40 Hz) resulted in reliable action potential output at 25-ms intervals (Fig. 3a). Across the population, FS and RS cells were driven with equally high reliability by light pulses at low frequencies (Fig. 3b). At higher frequencies, spike probability on each light cycle remained high for FS cells but decreased for RS cells.

Driving FS cells at 40 Hz caused a specific increase in the 35−40 Hz frequency band in the LFP (Fig. 3c and Supplementary Figs 5 and 6). We found that activation of FS cells in the 20−80 Hz range resulted in significant amplification of LFP power at those frequencies ($n = 14$ sites in 6 animals; Fig. 3d). However, activation of FS cells at lower frequencies did not affect LFP power, despite robust evoked FS firing on every light cycle. In contrast, 8−24 Hz light activation of RS cells in αCamKII−Cre mice induced increased LFP power at these frequencies, but RS activation at higher frequencies did not affect LFP power ($n = 13$ sites in 5 mice; Fig. 3d and Supplementary Fig. 5). Light stimulation in the untransduced contralateral barrel cortex did not affect LFP power at any frequency ($n = 6$ PV−Cre and 5 αCamKII−Cre animals; Supplementary Fig. 6).

This double dissociation of cell-type-specific state induction (gamma by FS and lower frequencies by RS) directly supports the prediction that FS-PV$^+$ interneuron activation is sufficient and specific for induction of gamma oscillations. To highlight this distinction, we compared the effects of stimulating the two cell types at 8 and 40 Hz. Stimulation of FS cells at 8 Hz in the PV−Cre mice had no effect on LFP power at 8 Hz, but FS stimulation at 40 Hz caused a significant increase in 40-Hz LFP power (paired t-test; $P < 0.001$; Fig. 3e). In contrast, stimulation of RS cells at 8 Hz in the αCamKII−Cre mice caused a significant increase of LFP power at 8 Hz ($P < 0.001$), whereas RS stimulation at 40 Hz caused only a small, nonsignificant increase in 40-Hz LFP power (Fig. 3f).

Gamma generation is a resonant circuit property

One possible explanation for these results is that increased FS firing recruits resonant gamma-range activity in the surrounding local network as a function of the synaptic and biophysical properties of the cortical circuit. Alternatively, the increase in gamma activity may result from the specific level of evoked FS spiking, and changing spiking probability would shift the frequency of the enhanced LFP band. To discriminate between these possibilities, we stimulated FS cells at varying levels of light intensity. We found that FS spike probability changed with light intensity such that the spike probability curve shifted laterally (Fig. 3g). Whereas drive affected the amplitude of enhancement, LFP power was selectively amplified within the gamma

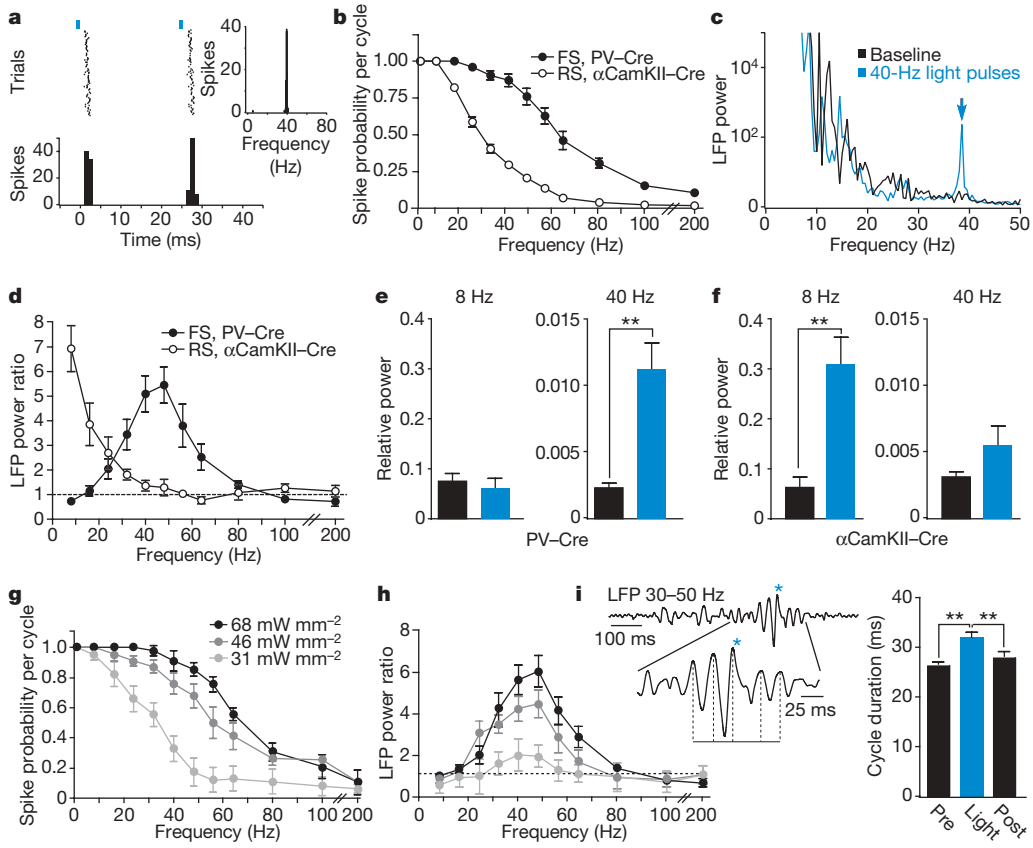

Figure 3 | FS inhibitory interneurons generate gamma oscillations in the local cortical network. **a**, In response to 40-Hz light pulses (blue bars), this FS cell fired reliably at 25-ms intervals, giving an instantaneous firing frequency of 40 Hz (inset). **b**, Average spike probability per light-pulse cycle in light-activated FS and RS cells in the PV−Cre and αCamKII−Cre mice, respectively (RS, $n = 17$, open circles; FS, $n = 22$, filled circles). **c**, Example of the increase in power at ~40 Hz in the LFP caused by activation of FS cells by light pulses at 40 Hz. **d**, Mean power ratio in each frequency band in response to light activation of FS (filled circles) and RS (open circles) cells at those frequencies. **e**, **f**, Comparison of the effect of activating FS and RS cells at 8 and 40 Hz on relative LFP power in those frequency bands. Black bars, relative power in the baseline LFP; blue bars, relative power in the presence of light pulses. **g**, Average spike probability of FS cells per light pulse cycle in response to three levels of light intensity. **h**, Mean power ratios from LFP recordings at the light intensity levels shown in **g**. **i**, The trace shows spontaneously occurring gamma activity in the LFP. Brief activation of FS cells (blue asterisk) prolonged the duration of the ongoing gamma cycle and consequently shifted the phase of the following cycles. The duration of the cycle during which the light stimulus was given (Light) was significantly longer than the preceding (Pre) or the following (Post) cycle. $^{**}P < 0.01$; error bars, mean ± s.e.m.

range regardless of light intensity or spike probability (Fig. 3h), indicating that the gamma oscillations evoked by FS activity are a resonant circuit property. In addition, randomly patterned light stimulation of FS cells with frequencies evenly distributed across a broad range evoked a significant increase in LFP power specific to the gamma range ($n = 7$ sites in 4 animals; $P < 0.05$; Supplementary Fig. 7), further indicating that FS-evoked gamma oscillations are an emergent property of the circuit and do not require exclusive drive in the gamma range.

Natural gamma oscillations require FS activity

To test whether intrinsically occurring gamma oscillations show a similar dependence on FS activity, we gave single light pulses during epochs of natural gamma. We found that brief FS activation shifted the phase of both spontaneously occurring gamma oscillations ($n = 26$ trials, 4 animals; Kruskal–Wallis test with Dunn's post-test; $P < 0.01$; Fig. 3i) and those evoked by midbrain reticular formation stimulation ($n = 18$ trials, 2 animals; $P < 0.05$; Supplementary Fig. 8). Furthermore, light-induced gamma oscillations were largely eliminated by blocking AMPA (α-amino-3-hydroxy-5-methyl-4-isoxazole propionic acid) and NMDA (*N*-methyl-D-aspartate) receptors, despite high levels of evoked FS firing ($n = 4$ sites in 4 animals; $P < 0.01$; Supplementary Fig. 9). These results indicate that induced gamma oscillations depend on rhythmic excitatory synaptic activity, as predicted by computational models of natural gamma oscillations and previous experiments[4,9,11,12,26]. In further agreement, spontaneous RS activity was entrained by 40 Hz FS stimulation, resulting in RS firing during the decay phase of the IPSP and preceding subsequent evoked FS spiking (Supplementary Fig. 10).

Evoked gamma phase regulates sensory processing

Gamma oscillations are thought to have a functional impact on cortical information processing by synchronizing the output of excitatory neurons[27,28]. This synchrony selects cell assemblies involved in a common task, such as encoding a sensory stimulus, and enhances their impact on downstream targets[27]. The cyclical FS inhibition underlying gamma oscillations is believed to cause this synchrony by rhythmically gating synaptic inputs[27,29]. Synaptic inputs arriving at the peak of inhibition should therefore produce a diminished response, but those arriving at the opposite phase in the gamma cycle should evoke a large response.

To test this hypothesis directly, we stimulated FS cells at 40 Hz with light pulses to establish gamma oscillations, and recorded the responses of RS cells to a single vibrissa deflection presented at one of five phases relative to a single gamma cycle ($n = 20$ cells in 3 animals; Fig. 4a). The timing of vibrissa-induced RS action potentials relative to light-evoked inhibition and the gamma cycle had a significant impact on the amplitude, timing and precision of the sensory-evoked responses of RS cells (Fig. 4b, c). The presence of gamma oscillations significantly decreased the amplitude of the RS sensory response at three phase points, consistent with the enhanced level of overall inhibition in this state ($P < 0.05$; 1-way ANOVA with Dunnett's post-test; Fig. 4d)[28]. Gamma phase also modulated the overall timing of the sensory response ($P < 0.01$; Fig. 4e), with spike latency delayed at phases 1−3 and unaffected at phases 4−5 (ref. 28). The precision of sensory-evoked spikes was significantly enhanced in a gamma-phase-dependent manner ($P < 0.01$; Fig. 4f). Our results indicate that the rhythmic, FS-induced IPSP restricts sensory transmission during its peak, and permits transmission after its decay, leading to a temporal sharpening of cortical sensory responses (Fig. 4g).

Our results provide the first causal demonstration of cortical oscillations induced by cell-type-specific activation. Synchronous FS-PV$^+$ interneuron activity driven by periodic stimulation of light-activated channels generated gamma oscillations in a cortical network, and these gated sensory processing in a temporally specific manner. These findings also demonstrate a unique application of optogenetic engineering in the *in vivo* brain for the study of discrete neuronal cell

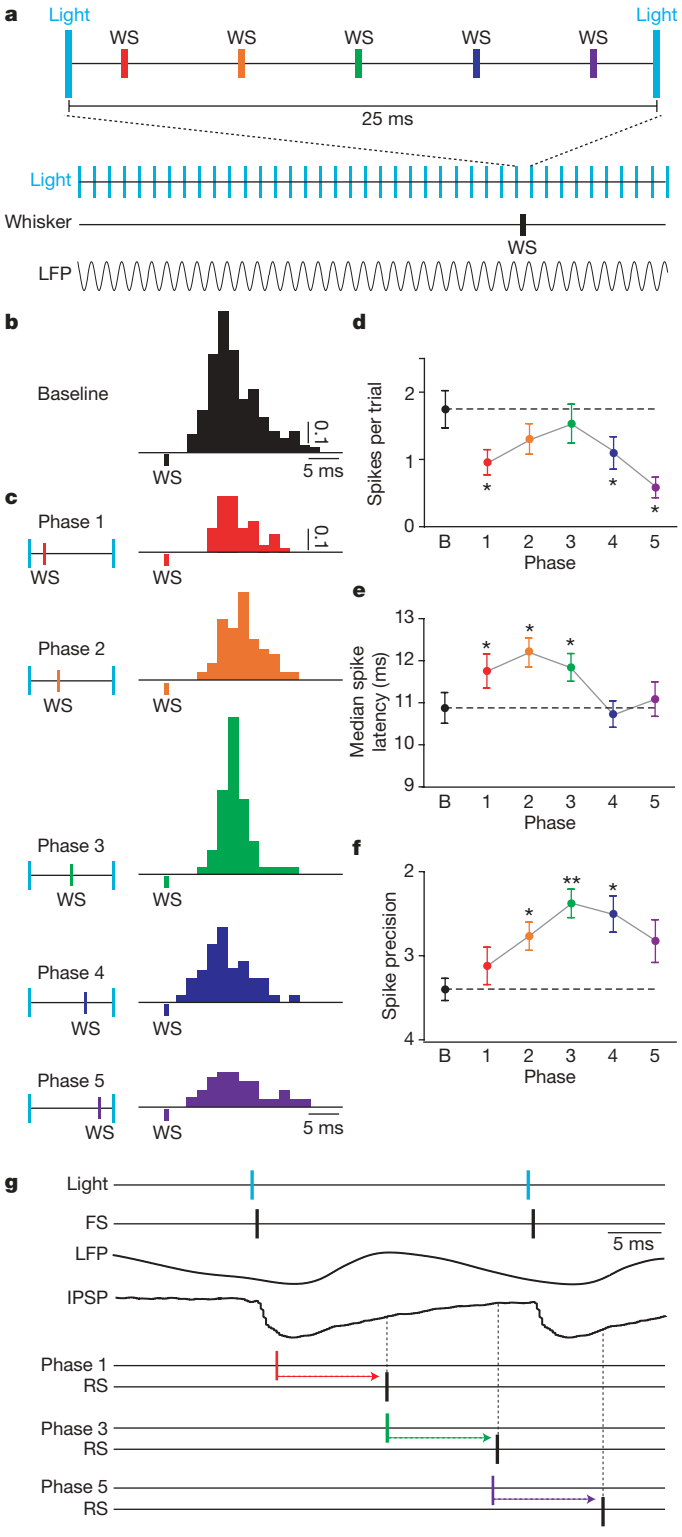

Figure 4 | Gamma oscillations gate sensory responses of excitatory neurons. **a**, In each trial, FS-PV$^+$ inhibitory interneurons were activated at 40 Hz and a single vibrissa deflection (whisker stimulus, WS) was presented at one of five phases. **b**, Baseline response of one layer 4 RS cell to single vibrissa deflections, shown in units of spikes per trial. **c**, Responses of the same cell when the whisker was deflected at each of five temporal phases relative to the induced gamma oscillation. **d**, Average spikes evoked per trial under each condition. Dotted line indicates baseline responses. **e**, Timing of the RS spike response, measured as median spike latency. **f**, Spike precision of the RS responses. **g**, Schematic model of the gating of sensory responses by gamma oscillations. IPSP and LFP examples are averaged data traces. $^*P < 0.05$, $^{**}P < 0.01$; error bars, mean ± s.e.m.

types under active network conditions. Future use of these techniques will allow direct testing of the impact of brain states on information processing in the behaving animal[30], and potentially the rescue of functional states in models of brain disease[31–33].

METHODS SUMMARY

AAV DIO *ChR2−mCherry* was injected into barrel cortex in adult PV−Cre[18] and CW2 (ref. 24) mice. Six days after injection, a subset of mice was perfused and tissue sectioned for immunohistochemistry to confirm the location, transduction efficiency and cell type specificity of ChR2 expression. Spread and immunohistochemical analysis of ChR2−mCherry expression was scored by hand through examination of every 30 μm coronal section for the presence of mCherry fluorescence. For electrophysiology, mice were anesthetized with isoflurane, and extracellular single-unit and LFP recordings were made in layers 2/3 and 4 of barrel cortex with tetrodes or stereotrodes. Intracellular recordings were made in the whole-cell configuration. Light pulses were given by means of an optical fibre positioned at the cortical surface directly above the recording site. For experiments using a broad range of light stimulation frequencies, we stimulated in bouts of 3 s at each frequency in a random order. For each stimulation frequency, we measured relative power in an 8 Hz band centred on that frequency. Relative power was calculated by measuring the ratio of power within the band of interest to total power in the power spectrum. To illustrate the impact of stimulation on the LFP, we also measured the ratio of power in a band with light stimulation to power in the band under baseline conditions. Vibrissae were stimulated by computer-controlled movements of piezoelectric wafers and consisted of single high-velocity deflections in the dorsal direction. For gamma-phase experiments, we gave a series of trials each consisting of a 1-s series of 1-ms light pulses at 40 Hz, with a single whisker deflection after the thirtieth light pulse. The precise timing of the whisker deflection relative to the light pulses was varied across five phase points. All numbers are given as mean ± s.e.m., except where otherwise noted.

Full Methods and any associated references are available in the online version of the paper at www.nature.com/nature.

Received 12 January; accepted 1 April 2009.
Published online 26 April 2009.

1. Berger, H. On the electroencephalogram of man. *Electroencephalogr. Clin. Neurophysiol.* **28** (Suppl.) 37–74 (1969).
2. Steriade, M. Grouping of brain rhythms in corticothalamic systems. *Neuroscience* **137,** 1087–1106 (2006).
3. Traub, R. D., Whittington, M. A., Stanford, I. M. & Jefferys, J. G. A mechanism for generation of long-range synchronous fast oscillations in the cortex. *Nature* **383,** 621–624 (1996).
4. Traub, R. D., Jefferys, J. G. & Whittington, M. A. Simulation of gamma rhythms in networks of interneurons and pyramidal cells. *J. Comput. Neurosci.* **4,** 141–150 (1997).
5. Whittington, M. A., Traub, R. D. & Jefferys, J. G. Synchronized oscillations in interneuron networks driven by metabotropic glutamate receptor activation. *Nature* **373,** 612–615 (1995).
6. Whittington, M. A., Faulkner, H. J., Doheny, H. C. & Traub, R. D. Neuronal fast oscillations as a target site for psychoactive drugs. *Pharmacol. Ther.* **86,** 171–190 (2000).
7. Deans, M. R., Gibson, J. R., Sellitto, C., Connors, B. W. & Paul, D. L. Synchronous activity of inhibitory networks in neocortex requires electrical synapses containing connexin36. *Neuron* **31,** 477–485 (2001).
8. Galarreta, M. & Hestrin, S. A network of fast-spiking cells in the neocortex connected by electrical synapses. *Nature* **402,** 72–75 (1999).
9. Hasenstaub, A. *et al.* Inhibitory postsynaptic potentials carry synchronized frequency information in active cortical networks. *Neuron* **47,** 423–435 (2005).
10. Wang, X. J. & Buzsaki, G. Gamma oscillation by synaptic inhibition in a hippocampal interneuronal network model. *J. Neurosci.* **16,** 6402–6413 (1996).
11. Borgers, C., Epstein, S. & Kopell, N. J. Background gamma rhythmicity and attention in cortical local circuits: a computational study. *Proc. Natl Acad. Sci. USA* **102,** 7002–7007 (2005).
12. Whittington, M. A., Traub, R. D., Faulkner, H. J., Stanford, I. M. & Jefferys, J. G. Recurrent excitatory postsynaptic potentials induced by synchronized fast cortical oscillations. *Proc. Natl Acad. Sci. USA* **94,** 12198–12203 (1997).
13. Gray, C. M. & Singer, W. Stimulus-specific neuronal oscillations in orientation columns of cat visual cortex. *Proc. Natl Acad. Sci. USA* **86,** 1698–1702 (1989).
14. Fries, P., Reynolds, J. H., Rorie, A. E. & Desimone, R. Modulation of oscillatory neuronal synchronization by selective visual attention. *Science* **291,** 1560–1563 (2001).
15. Fries, P., Nikolic, D. & Singer, W. The gamma cycle. *Trends Neurosci.* **30,** 309–316 (2007).
16. Boyden, E. S., Zhang, F., Bamberg, E., Nagel, G. & Deisseroth, K. Millisecond-timescale, genetically targeted optical control of neural activity. *Nature Neurosci.* **8,** 1263–1268 (2005).
17. Deisseroth, K. *et al.* Next-generation optical technologies for illuminating genetically targeted brain circuits. *J. Neurosci.* **26,** 10380–10386 (2006).
18. Hippenmeyer, S. *et al.* A developmental switch in the response of DRG neurons to ETS transcription factor signaling. *PLoS Biol.* **3,** e159 (2005).
19. Kuhlman, S. J. & Huang, Z. J. High-resolution labeling and functional manipulation of specific neuron types in mouse brain by Cre-activated viral gene expression. *PLoS ONE* **3,** e2005 (2008).
20. Ascoli, G. A. *et al.* Petilla terminology: nomenclature of features of GABAergic interneurons of the cerebral cortex. *Nature Rev. Neurosci.* **9,** 557–568 (2008).
21. Ren, J. Q., Aika, Y., Heizmann, C. W. & Kosaka, T. Quantitative analysis of neurons and glial cells in the rat somatosensory cortex, with special reference to GABAergic neurons and parvalbumin-containing neurons. *Exp. Brain Res.* **92,** 1–14 (1992).
22. Markram, H. *et al.* Interneurons of the neocortical inhibitory system. *Nature Rev. Neurosci.* **5,** 793–807 (2004).
23. Cauli, B. *et al.* Molecular and physiological diversity of cortical nonpyramidal cells. *J. Neurosci.* **17,** 3894–3906 (1997).
24. Zeng, H. *et al.* Forebrain-specific calcineurin knockout selectively impairs bidirectional synaptic plasticity and working/episodic-like memory. *Cell* **107,** 617–629 (2001).
25. Hubbard, J. I., Llinas, R. & Quastel, D. M. J. *Electrophysiological Analysis of Synaptic Transmission* (The Camelot Press Ltd, 1969).
26. Borgers, C. & Kopell, N. Effects of noisy drive on rhythms in networks of excitatory and inhibitory neurons. *Neural Comput.* **17,** 557–608 (2005).
27. Engel, A. K. & Singer, W. Temporal binding and the neural correlates of sensory awareness. *Trends Cogn. Sci.* **5,** 16–25 (2001).
28. Fries, P., Neuenschwander, S., Engel, A. K., Goebel, R. & Singer, W. Rapid feature selective neuronal synchronization through correlated latency shifting. *Nature Neurosci.* **4,** 194–200 (2001).
29. Burchell, T. R., Faulkner, H. J. & Whittington, M. A. Gamma frequency oscillations gate temporally coded afferent inputs in the rat hippocampal slice. *Neurosci. Lett.* **255,** 151–154 (1998).
30. Huber, D. *et al.* Sparse optical microstimulation in barrel cortex drives learned behaviour in freely moving mice. *Nature* **451,** 61–64 (2008).
31. Orekhova, E. V. *et al.* Excess of high frequency electroencephalogram oscillations in boys with autism. *Biol. Psychiatry* **62,** 1022–1029 (2007).
32. Spencer, K. M., Niznikiewicz, M. A., Shenton, M. E. & McCarley, R. W. Sensory-evoked gamma oscillations in chronic schizophrenia. *Biol. Psychiatry* **63,** 744–747 (2008).
33. Uhlhaas, P. J., Haenschel, C., Nikolic, D. & Singer, W. The role of oscillations and synchrony in cortical networks and their putative relevance for the pathophysiology of schizophrenia. *Schizophr. Bull.* **34,** 927–943 (2008).

Supplementary Information is linked to the online version of the paper at www.nature.com/nature.

Acknowledgements We are grateful to S. Arber for the PV−Cre mice, S. Tonegawa for the CW2 mice, and A. Bradshaw, C. Ruehlmann and S. Su for technical assistance. We thank members of the Boyden laboratory and J. Bernstein for help in setting up optical techniques. We thank members of the Tsai and Moore laboratories, D. Vierling-Claassen and M. J. Higley for discussions and comments on the paper. This study was supported by grants from Tom F. Petersen, the NIH and the NSF to C.I.M. and by the Simons Foundation Autism Research Initiative to L.-H.T. K.D. is supported by the NIH Pioneer Program. L.-H.T. is an investigator of the Howard Hughes Medical Institute. J.A.C. is supported by a K99 from the NIH/NEI, M.C. and K.M. by postdoctoral fellowships from the Knut och Alice Wallenberg Foundation, M.C. by a NARSAD Young Investigator Award, and F.Z. by an NIH NRSA.

Author Contributions J.A.C., M.C., K.M., L.-H.T. and C.I.M. designed the experiments. F.Z. and K.D. designed and cloned the AAV DIO ChR2−mCherry vector. M.C. and K.M. characterized the virus *in vitro* and *in vivo* and injected the animals. M.C. performed histological statistical analyses. J.A.C. performed and analysed the extracellular recordings. U.K. and J.A.C. performed the intracellular recordings. U.K. analysed the intracellular data. J.A.C., M.C., K.M., U.K., L.-H.T. and C.I.M. wrote the manuscript.

Author Information Reprints and permissions information is available at www.nature.com/reprints. Correspondence and requests for materials should be addressed to C.I.M. (cim@mit.edu), L.-H.T (lhtsai@mit.edu) or K.D. (deissero@stanford.edu).

METHODS

Animals. All procedures were conducted in accordance with the National Institutes of Health guidelines and with the approval of the Committee on Animal Care at MIT. PV−Cre ($n = 21$) and CW2 ($n = 7$) mice were 6−12 weeks old at the time of viral injections. Electrophysiological recordings and immunohistochemical analyses were performed 1−3 weeks after viral injections.

AAV vectors. ChR2 fused to the fluorescent protein mCherry was cloned in antisense direction into pAAV-MCS (Stratagene) to create AAV DIO *ChR2−mCherry* (Fig. 1a and Supplementary Fig. 1; for vector outline and sequence see www.optogenetics.org). *ChR2−mCherry* was flanked by a pair of canonical *loxP* sites and a pair of mutated *lox2272* sites. A woodchuck hepatatis B virus post-transcriptional element was placed in sense direction 5′ of the poly(A). Adeno-associated viral particles of serotype 2 were produced by the Vector Core Facility at The University of North Carolina at Chapel Hill.

Virus injections. Adult PV−Cre[18] or CW2 (ref. 24) mice were anesthetized with an intraperitoneal injection of a mixture of ketamine (1.1 mg kg^{-1}) and xylazine (0.16 mg kg^{-1}). A small craniotomy was made 1.5 mm posterior to bregma and 3.0 mm lateral to the midline. Virus was delivered through a small durotomy by a glass micropipette attached to a Quintessential Stereotaxic Injector (Stoelting). The glass micropipette was lowered to 0.4 mm below the cortical surface. A bolus of 0.5 µl of virus (AAV DIO *ChR2−mCherry*; 2×10^{12} viral molecules per ml) was injected into barrel cortex at 0.1 µl min^{-1}. The pipette was then retracted to a depth of 250 µm below the surface and an additional 0.5 µl virus was injected at the same rate. The pipette was held in place for 5 min after the injection before being retracted from the brain. The scalp incision was sutured, and post-injection analgesics were given to aid recovery (0.1 mg kg^{-1} Buprenex).

Immunohistochemistry. Mice were transcardially perfused with 100 mM PBS followed by 4% formaldehyde in PBS, and brains were post-fixed for 18 h at 4 °C. Free-floating sections (30 µm) were cut using a vibratome (Leica VT100) and incubated with blocking solution (10% donkey serum in PBS with 0.3% Triton-X 100) for 1 h at room temperature (20 °C) and then incubated at room temperature overnight with primary antibody diluted in blocking solution. The following primary antibodies were used: NeuN (Chemicon; 1:1,000), parvalbumin PVG-214 (Swant; 1:2,000), GABA (Sigma; 1:4,000) and CamKII (Epitomics; 1:500). After washing, antibody staining was revealed using species-specific fluorophore-conjugated secondary antibodies (Cy5 from Jackson Laboratories, Alexa 488 from Molecular Probes). GABA was detected with biotinylated secondary antibodies (Jackson Laboratories) and revealed using a combination of ABC kit (Vector Laboratories) and TSA fluorescent amplification kit (Perkin-Elmer). Sections were mounted on glass slides with Vectashield (Vector Laboratories) and coverslipped.

Quantification. Spread and labelling efficiency were scored by hand by examination of every 30 µm coronal section ($n = 3$ animals per genotype) for the presence of mCherry fluorescence using a Zeiss LSM510 confocal microscope. For quantification of co-labelling of ChR2−mCherry and PV ($n = 4$ animals per genotype) confocal images were acquired and individual cells were identified independently for each of the two fluorescent channels. Scans from each channel were collected in multi-track mode to avoid cross-talk between channels.

Electrophysiology. Mice were anesthetized with isoflurane and held in place with a head post cemented to the skull. All incisions were infiltrated with lidocaine. A small craniotomy was made over barrel cortex approximately 200 µm anterior to the virus injection site. Extracellular single-unit and LFP recordings were made with tetrodes or stereotrodes. Intracellular recordings were conducted by whole-cell *in vivo* recording in current clamp mode. Stimulus control and data acquisition was performed using software custom-written in LabView (National Instruments) and Matlab (The Mathworks). Further electrophysiology methods and a description of the reversal potential calculation are given in Supplementary Methods.

Light stimulation was generated by a 473 nm laser (Shanghai Dream Lasers) controlled by a Grass stimulator (Grass Technologies) or computer. Light pulses were given via a 200-µm diameter, unjacketed optical fibre (Ocean Optics) positioned at the cortical surface 75−200 µm from the recording electrodes. For experiments using the broad range of light-stimulation frequencies (8, 16, 24, 32, 40, 48, 80, 100 and 200 Hz), we stimulated in bouts of 3 s of 1-ms pulses at 46 mW mm^{-2} at each frequency in a random order. In a subset of these experiments, we stimulated at 31, 46 and 68 mW mm^{-2}.

Vibrissae were stimulated by computer-controlled movements of piezoelectric wafers (Piezo Systems). Vibrissa stimulations were single high-velocity deflections in the dorsal and then in the ventral direction (~6 ms duration). In most cases, adjacent vibrissae that yielded indistinguishable amplitude responses during hand mapping were deflected simultaneously. Vibrissa stimulations evoked layer 4 RS spike responses with an onset latency of 9.1 ± 0.08 ms. For RS cell response suppression experiments, light pulses were given on randomly interleaved trials. For gamma-phase experiments, we gave a series of trials each consisting of a 1-s series of 1-ms light pulses at 40 Hz, with a single whisker deflection after the thirtieth light pulse. The precise timing of the whisker deflection relative to the light pulses was varied across five phase points. Each of the five phase points was included in a random order across a minimum of 250 total trials.

Unit and LFP analysis used software custom-written in Igor Pro (Wavemetrics). For each stimulation frequency, we measured the relative power in an 8-Hz band centred on that frequency. For each recording site, we measured power from 5−10 LFP traces under each condition. Example power spectra are averages of the power spectra from 5−10 traces of unfiltered LFPs from individual experiments. Relative power was calculated by measuring the ratio of power within the band of interest to total power in the power spectrum of the unfiltered LFP. We also measured the power ratio: $P_{light}/P_{baseline}$, where P_{light} is the relative power in a frequency band in the presence of light stimulation and $P_{baseline}$ is the power in that band in the absence of light stimulation. All numbers are given as mean ± s.e.m., except where otherwise noted.